NANO LETTERS

Letter

pubs.acs.org/NanoLett

Synaptic Plasticity Selectively Activated by Polarization-Dependent Energy-Efficient Ion Migration in an Ultrathin Ferroelectric Tunnel Junction

Chansoo Yoon,[†] Ji Hye Lee,[†] Sangik Lee,[†] Ji Hoon Jeon,[†] Jun Tae Jang,[‡] Dae Hwan Kim,[‡] Young Heon Kim,[§] and Bae Ho Park*[,†]

[†]Division of Quantum Phases & Devices, Department of Physics, Konkuk University, Seoul 143-701, Korea

[‡]School of Electrical Engineering, Kookmin University, Seoul 136-702, Korea

[§]Korea Research Institute of Standards and Science, Daejeon 305-304, Korea

S *Supporting Information*

ABSTRACT: Selectively activated inorganic synaptic devices, showing a high on/off ratio, ultrasmall dimensions, low power consumption, and short programming time, are required to emulate the functions of high-capacity and energy-efficient reconfigurable human neural systems combining information storage and processing (Li et al. *Sci. Rep.* **2014**, *4*, 4096). Here, we demonstrate that such a synaptic device is realized using a Ag/$PbZr_{0.52}Ti_{0.48}O_3$ (PZT)/$La_{0.8}Sr_{0.2}MnO_3$ (LSMO) ferroelectric tunnel junction (FTJ) with ultrathin PZT (thickness of ∼4 nm). Ag ion migration through the very thin FTJ enables a large on/off ratio (10^7) and low energy consumption (potentiation energy consumption = ∼22 aJ and depression energy consumption = ∼2.5 pJ). In addition, the simple alignment of the downward polarization in PZT selectively activates the synaptic plasticity of the FTJ and the transition from short-term plasticity to long-term potentiation.

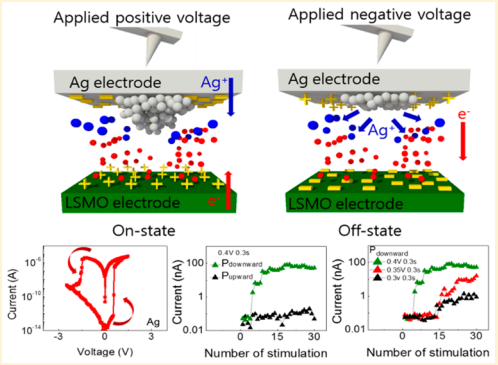

KEYWORDS: *Ultrathin ferroelectric film, synaptic device, low energy consumption, giant on/off ratio, selective activation*

Synapses play the key role in neuromorphic computing by varying the connection weight between two neurons, the so-called synaptic plasticity.[1−3] Neuroplasticity underlying the brain ability to memorize can be categorized into short-term plasticity (STP) and long-term potentiation (LTP), which are respectively achieved through temporal and permanent enhancement of a synaptic connection.[4] The memristor with a gradually modified conductance is applicable to emulating neuromorphic computing conducted using biological syanpses.[5−9] Low energy consumption and ultrasmall dimension are required for a synaptic memristor device because an enormous number of 10^{15} synapses in human brain only consume ∼10 W per synaptic event with duration of ∼100 ms.[2] Furthermore, the synaptic plasticity in neurons can be dynamically modulated by astrocyte, which might reconfigure circuits between neurons.[10−13]

A two-terminal ferroelectric tunnel junction (FTJ), where gradual conductance modulation is accompanied by change in the ferroelectric domain configuration, is considered as a synaptic device with low energy consumption.[2,14−18] However, the transition between STP and LTP due to stimulation has not been reported in FTJ-based synaptic devices. In addition, the on/off ratio of an FTJ is much smaller than that of a conventional resistive switching device, such as a conductive-bridge memory device.[19,20]

A conductive-bridge memory device, where a conductive bridge can be repeatedly formed and broken by fast diffusion and migration of cations,[19−21] mimics the biological potentiation and depression of the synapse.[4,6,21−25] However, a conductive-bridge memory-based synaptic device has not shown selective activation of synaptic behavior without the aid of an external selection device. Because ferroelectric polarization generates an internal electric field, the reversal of ferroelectric polarization can provide a simple way to change in cation migration inside FTJ. Therefore, combining the reversal of nonvolatile ferroelectric polarization and fast migration of cations can facilitate selection, memory, and learning functions in a single device leading to implementation of a selectively activated inorganic synaptic device with a high on/off ratio, ultrasmall dimension, low power consumption, and short programming time.

Here, we report a new single synaptic Ag/$PbZr_{0.52}Ti_{0.48}O_3$ (PZT)/$La_{0.8}Sr_{0.2}MnO_3$ (LSMO) device whose ultrathin ferroelectric PZT layer (∼4 nm) serves as a selective electrolyte for cation migration. It reveals a large on/off ratio (10^7) and low energy consumption (potentiation energy consumption = ∼22

Received: December 22, 2016
Published: February 23, 2017

DOI: 10.1021/acs.nanolett.6b05308
Nano Lett. 2017, 17, 1949−1955

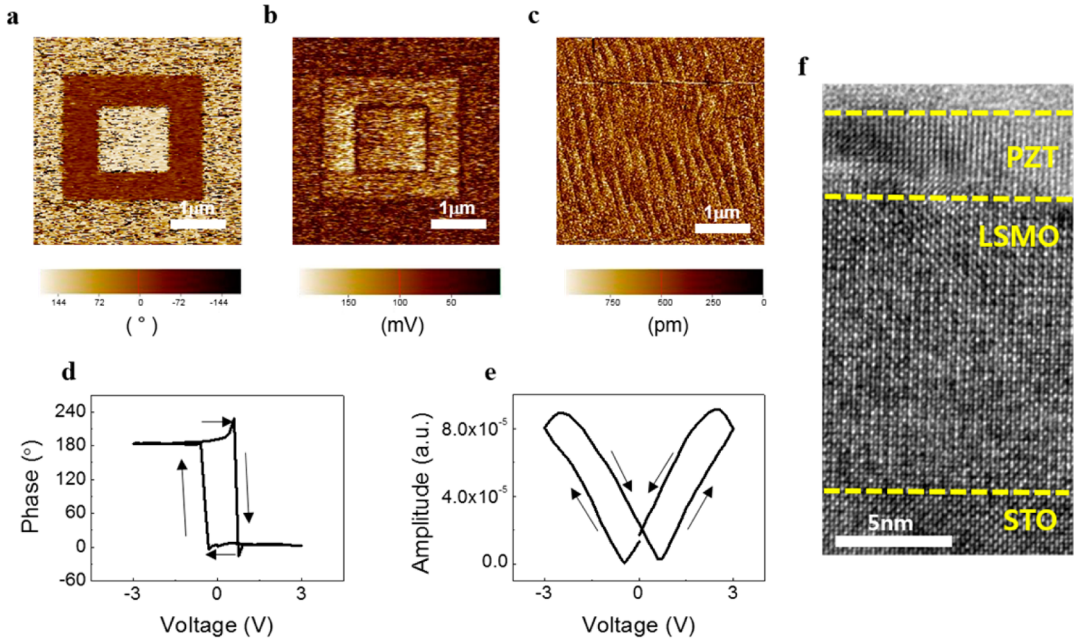

Figure 1. Local ferroelectric and structural properties of an ultrathin PZT film on LSMO/STO. (a–c) PFM out-of-plane phase (a), PFM out-of-plane amplitude (b), and AFM topography (c) images obtained on a PZT/LSMO/STO heterostructure with an ultrathin PZT layer (~4 nm) after applying an external voltage of 2.1 V to a square of 3 × 3 μm^2 and then −2.1 V to a square of 1.5 × 1.5 μm^2 inside it. (d and e) Hysteretic behaviors of the PFM phase (d) and amplitude (e) signals measured on a Pt/PZT/LSMO heterostructure with 0.6 × 0.6 μm^2 area as functions of applied bias. (f) Cross-sectional HR-TEM image of the PZT/LSMO/STO heterostructure.

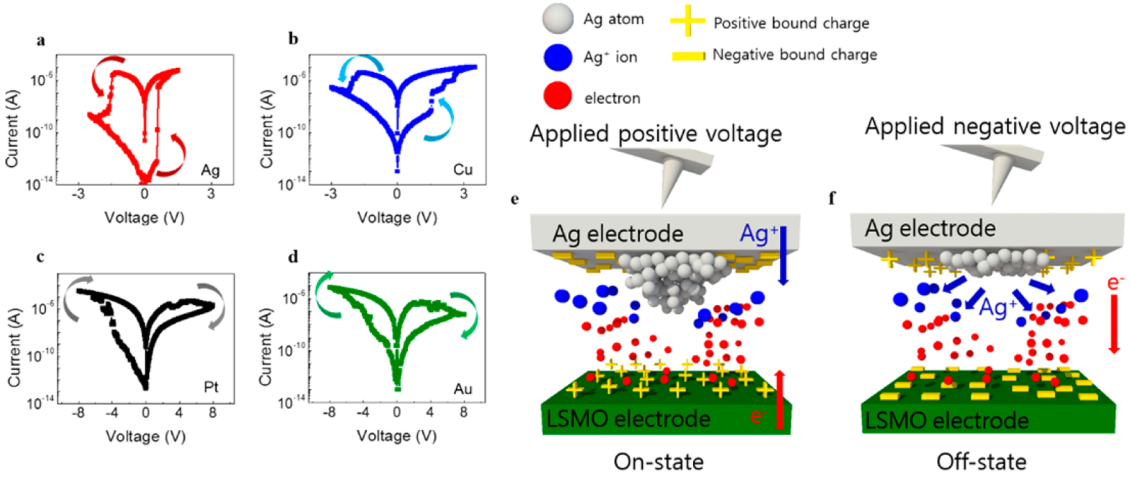

Figure 2. Resistive switching behavior depending on the top electrode material. (a–d) Typical bipolar resistive switching curves of top electrode (TE)/PZT/LSMO FTJs where TE is Ag (a), Cu (b), Pt (c), or Au (d). (e and f) Schematic illustrations of cation migration and resulting electrochemical reaction in a FTJ at low (e) and high (f) resistance states.

aJ and depression energy consumption = ~2.5 pJ) ascribed to modulation of the tunneling barrier width by Ag ion migration through the ultrathin FTJ, which is driven by both external voltage and polarization bound charges. It also shows synaptic plasticity and transition from STP to LTP, which is selectively activated by bound charges near the Ag/PZT interface: negative and positive bound charges near the Ag/PZT interface activate and inactivate synaptic potentiation, respectively. Therefore, our Ag/PZT/LSMO structure offers an energy-efficient, ultrasmall, and wide-range operating single synaptic device whose activation is controlled by the polarization direction selectively and randomly.

Figure 1a and b shows the out-of-plane piezoresponse force microscopy (PFM) phase and the amplitude images, respectively, of a PZT/LSMO heterostructure grown on a $SrTiO_3$ (STO) substrate. Before obtaining the images, an external voltage of 2.1 V was applied to a square of 3 × 3 μm^2, and then −2.1 V was applied to a square of 1.5 × 1.5 μm^2 inside it using a conductive atomic force microscopy (AFM) tip. The PFM phase image reveals dark and bright contrasts in the outer (3 × 3 μm^2) and inner (1.5 × 1.5 μm^2) squares, respectively, indicating that the two squares have opposite ferroelectric polarization directions. Similar contrasts of the two squares observed in the PFM amplitude image indicate that the two squares have nearly equal amplitudes of polarization. However, the applied voltage does not induce a change in the surface morphology, as shown in the AFM topography image (Figure 1c) obtained after applying the external voltage. The terrace-

DOI: 10.1021/acs.nanolett.6b05308
Nano Lett. 2017, 17, 1949–1955

like structures in the AFM topography image are typical features of epitaxial films grown in the layer-by-layer mode, which conform to their substrates. We also investigated the local out-of-plane ferroelectric characteristics of our PZT film by measuring hysteretic behaviors of the PFM phase and the amplitude at a specific point on a Pt/PZT/LSMO heterostructure, as shown in Figure 1d and e. The top Pt electrode with 0.6 × 0.6 μm^2 area was used to reduce contact resistance between a conductive AFM tip and the heterostructure. Coercive voltages of −0.5 and 0.6 V are determined from the minima of the amplitude loop, which are in accord with the voltages where sudden changes in the phase loop occur. The ferroelectricity of the PZT film is verified by the local hysteretic behaviors in Figure 1d and e as well as PFM images (Figure 1a and b) showing the areas with opposite polarization directions controlled by the external voltage. We probed crystallinity and epitaxial growth of our PZT/LSMO heterostructure using a high-resolution transmission electron microscopy (HR-TEM) cross-section image (Figure 1f). The epitaxial growth of both PZT and LSMO films is demonstrated by the well-aligned lattices in the HR-TEM image. The thickness of the PZT film is estimated to be approximately 4 nm from the image.

In order to measure resistive switching behavior, we fabricated Ag top electrodes on the PZT/LSMO heterostructure. The Ag/PZT/LSMO device exhibits a bipolar resistive switching behavior in the current−voltage (I−V) curve, where set (from off to on) and reset (from on to off) switchings respectively occur at positive and negative voltages (Figure 2a). It shows a remarkably higher on/off ratio (10^7) than those (10^4−10^5) of recently reported FTJs at room temperature,[15,26] which may be caused by Ag ion migration through the very thin PZT layer with ferroelectric polarization.

If a positive bias is applied to an Ag top electrode, ferroelectric polarization underneath it tends to be directed downward, and negative bound charges move to the Ag/PZT top interface (Figure 2e).[26] Owing to the electric field caused by both external positive bias applied to the top Ag electrode and negative bound charges accumulated at the Ag/PZT interface, the positive Ag ions, originating from the oxidation of Ag anode, can be collected near the Ag/PZT interface. Then the Ag ions can be reduced back to Ag atoms by free electrons passing through the PZT layer because ionic conductivity is very low in an oxide−electrolyte and the current through it mainly consists of electron current.[20,27,28] With the continuation of the oxidation/reduction processes, the successive accumulation of Ag atoms at the Ag/PZT interface leads to the nucleation and extension of the Ag conducting filament at some local region of the Ag electrode surface. However, the growth of conducting filament is very slow down near the PZT/LSMO interface because positive Ag ions are repelled by positive bound charges from downward polarization. As a result, the ferroelectric barrier width becomes thinner by the migrated Ag ions leading to a higher tunneling transmittance and switching to a low resistance on-state of the Ag/PZT/LSMO device.[6,26] The I−V curves of our Ag/PZT/LSMO device in both on- and off-states were well fitted using a direct tunneling function (Supporting Information, Figure S3) while those of conductive-bridge-based resistive switching respectively showed Ohmic[29] (on-state) and tunneling[30] (off-state) behaviors. We used the current density J given by Gruverman et al.[31] for a trapezoidal potential barrier (Brinkman model)[32] based on the Wentzel−Kramers−Brillouin (WKB) approximation. From the fitting results, we found that the tunneling barrier width was reduced by 0.7 nm after set switching (Supporting Information, Figure S3). This indicated that the migrated Ag ions of our Ag/PZT/LSMO did not form a complete Ag conducting filament but reduced the tunneling barrier width in on-state (Supporting Information, Figure S3).

On the other hand, when a negative bias applied to the Ag top electrode, the rupture of the Ag conducting filament takes place due to a thermal-assistant electrochemical reaction (Figure 2f).[20,27,28] The front of the conducting filament has the thinnest cross-sectional area and then the highest current density leading to high temperature in there. Under the negative voltage applied to the Ag top electrode, the oxidation reaction at the front of the conducting filament will be accelerated by high temperature resulting in the dissolution of the conducting protrusion. Then, the tunneling barrier width becomes thicker, and the device switches back to a high resistance off-state. Because the off-state current passed not through a confined Ag conducting filament but through the whole area under the top electrode, it showed the dependence on the electrode size[33] (Supporting Information, Figure S5). However, the on-state current did not depend on the electrode size probably because positive Ag ion migration reduced the tunneling barrier width inhomogeneously under the top electrode. The contribution of Ag ion migration to conductance was experimentally demonstrated by temperature-dependent resistive switching behaviors (Supporting Information, Figure S6). Both on- and off-state resistance versus temperature curves were well-fitted by the Arrhenius equation. Furthermore, the estimated activation energy for Ag ion migration significantly decreased after ferroelectric polarization in the PZT was aligned to downward direction.

For comparison, we also fabricated Cu/PZT/LSMO, Pt/PZT/LSMO, and Au/PZT/LSMO devices where Cu ions are fast diffusive ions while Pt and Au ions are not. The Cu/PZT/LSMO device (Figure 2b) reveals similar bipolar behavior to that of the Ag/PZT/LSMO indicating that migration of positive Cu ions modulates the width of the tunneling barrier. The off-state current of the Cu/PZT/LSMO device is higher than that of the Ag/PZT/LSMO implying that the barrier height at Cu/PZT is smaller than that at Ag/PZT. In contrast, the on-state current of the Cu/PZT/LSMO device is similar to that of the Ag/PZT/LSMO device. The on-state current is determined when the growth rate of conducting filament is balanced with its thermal-assisted rupture rate which strongly depends on temperature increase by Joule heating. Therefore, our data indicate that the Ag and Cu filaments have similar resistance values leading to similar Joule heating effects. However, the Pt/PZT/LSMO (Figure 2c) and Au/PZT/LSMO (Figure 2d) devices exhibit opposite switching direction to that of the Ag/PZT/LSMO, which cannot be explained by migration of positive Pt and Au ions originating from the Pt and Au top electrodes, respectively. The opposite switching direction observed in Au/PZT/LSMO and Pt/PZT/LSMO can be explained by polarization reversal and resulting modulation of the PZT/LSMO interface: upward and downward ferroelectric polarizations in the thin PZT film induce hole accumulation (on-state) and depletion (off-state) at the PZT/LSMO interface, respectively, where LSMO is a hole-doped material.[34] It seems that, for Ag/PZT/LSMO and Cu/PZT/LSMO, the effect of Ag and Cu ion migration overwhelms the effect of modulation at the PZT/LSMO interface. In addition, the resistive switching voltages of Pt/PZT/LSMO and Au/PZT/LSMO were similar to the coercive voltages of their PFM

DOI: 10.1021/acs.nanolett.6b05308
Nano Lett. 2017, 17, 1949−1955

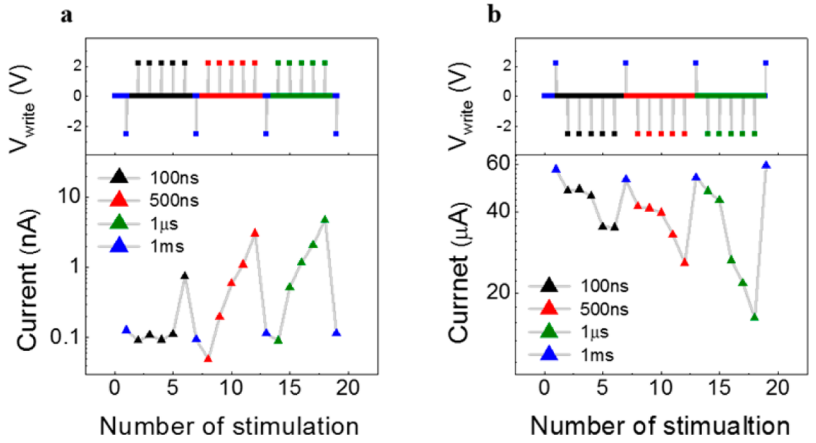

Figure 3. Potentiation and depression of an Ag/PZT/LSMO FTJ. (a and b) Dependence of potentiation (a) and depression (b) on the duration (100 ns, 500 ns, and 1.0 μs) of positive and negative pulses whose amplitudes were fixed at 2.2 V and −2.5 V, respectively.

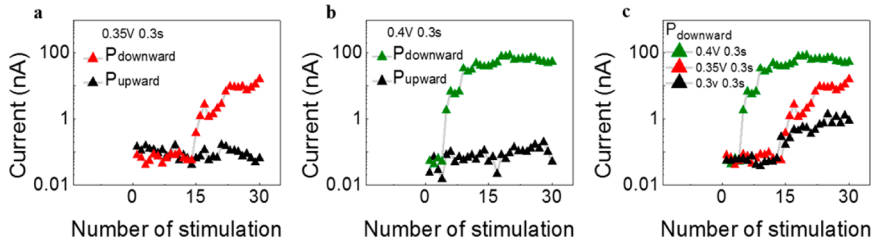

Figure 4. Selectively activated synaptic plasticity of an Ag/PZT/LSMO FTJ. (a and b) Gradual modulation of the current passing through an Ag/PZT/LSMO by consecutive positive pulses with 0.35 V amplitude and 0.3 s duration (a) and with 0.4 V amplitude and 0.3 s duration (b) at downward and upward polarizations. (c) Dependence of the gradual current modulation on the pulse amplitude and duration at downward polarization.

phase hysteresis loops (Supporting Information, Figure S7). Therefore, we can expect that resistive switching of Pt/PZT/LSMO and Au/PZT/LSMO originates from polarization reversal-induced hole carrier density modulation at the PZT/LSMO interface. An Ag/PZT/LSMO device, when negative bias sweeping was performed before Ag ion migration was triggered, also showed similar set switching originating from polarization reversal-induced hole carrier density modulation at the PZT/LSMO interface (Supporting Information, Figure S8). However, after the successive positive sweeping was carried out, additional set switching was observed, and the device showed resistive switching induced by Ag ion migration (Supporting Information, Figure S8).

According to the aforementioned mechanism, we expected that gradual change in direct tunneling current of the Ag/PZT/LSMO was enabled by barrier width control originating from Ag ion migration. For potentiation, we applied five consecutive stimulation positive pulses with a fixed amplitude (2.2 V) and variable durations (100 ns, 500 ns, and 1.0 μs) after rendering the device off using a negative pulse with an amplitude of −2.5 V and a duration of 1.0 ms (Figure 3a). A reading pulse with an amplitude of 0.2 V and a duration of 10 ms was applied to measure the current level just after applying each programming voltage pulse. For depression, we applied five consecutive stimulation negative pulses with a fixed amplitude (−2.5 V) and variable durations (100 ns, 500 ns, and 1.0 μs) after rendering the device on using a positive pulse with an amplitude of 2.2 V and a duration of 1.0 ms (Figure 3b). Remarkably, both potentiation and depression of our Ag/PZT/LSMO device can be induced by extremely short stimulation pulses with a duration of 100 ns. Such a short programming time may be caused by Ag ion migration and electrochemical reaction confined in a very short distance (<nm), which are enabled by the combination of applied voltage and polarization bound charges, near the Ag/PZT interface. Therefore, we achieve considerably low programming energy (potentiation energy consumption = ~22 aJ and depression energy consumption = ~2.5 pJ) by minimizing the programming time. These energies are much lower than those (potentiation energy consumption = 0.1 pJ to 0.1 nJ and depression energy consumption = 0.1 nJ to 0.1 μJ) of previously reported conductive-bridge memory-based synaptic devices,[1,4,6,8,9,25] which showed longer programming times and higher current levels than ours.

In order to explore the relationship between Ag ion migration and ferroelectric polarization direction in the thin PZT film, we compared potentiation behaviors at opposite polarization directions. External voltages of 3.0 V and −3.0 V were applied to the Ag electrode with 1.1 × 1.1 μm^2 area for achieving downward and upward polarizations in the thin PZT film, respectively. For the case of downward polarization, we applied successive 50 negative pulses with an amplitude of −0.3 V and a duration of 0.5 s to obtain an off-state without polarization reversal in the Ag/PZT/LSMO capacitor (Supporting Information, Figure 10). Afterward, we applied consecutive stimulation positive pulses with (amplitude, duration) of (0.35 V, 0.3 s) and (0.4 V, 0.3 s), respectively, whose amplitudes are smaller than both coercive and set voltages of PZT. As shown using the black triangle dots in Figure 4a and b, the current levels are gradually increased by both consecutive stimulation voltage pulses at the downward polarization in the thin PZT film. In contrast, the red and green triangle dots in Figure 4a and b reveal that such consecutive

DOI: 10.1021/acs.nanolett.6b05308
Nano Lett. 2017, 17, 1949−1955

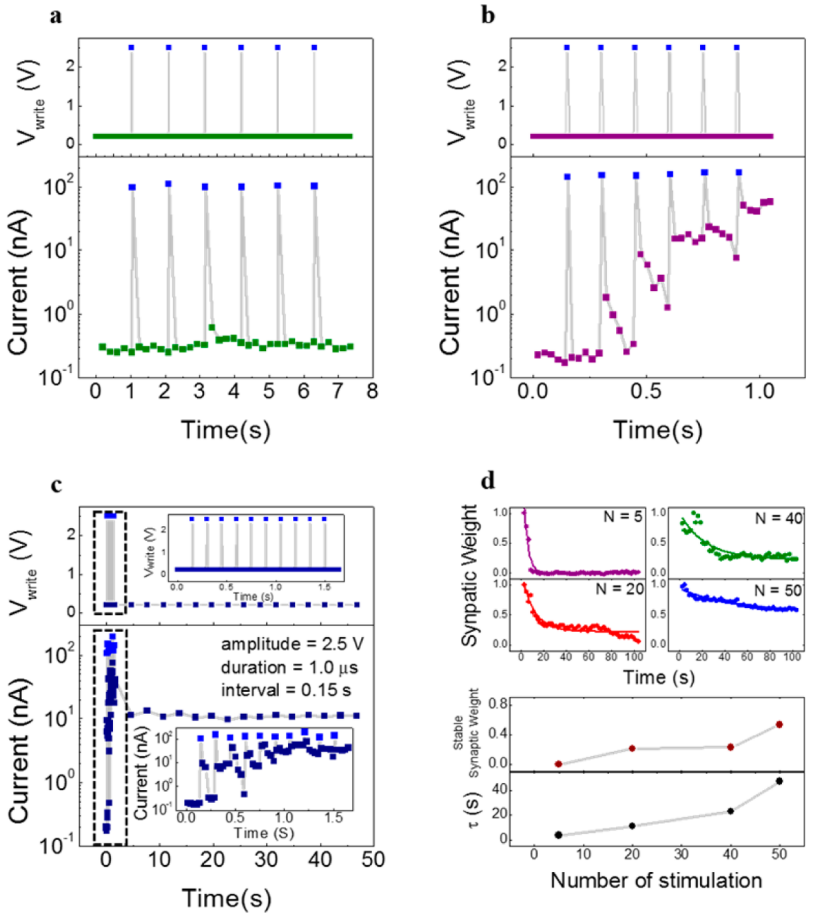

Figure 5. Synaptic plasticity and its stability in an Ag/PZT/LSMO FTJ. (a and b) STP (a) and LTP (b) in an Ag/PZT/LSMO FTJ, which were induced by positive pulses (2.5 V amplitude and 100 ns duration) with intervals of 1.0 and 0.15 s, respectively. (c) Time evolution of the log-scale current level during and after applying 10 stimulation pulses (2.5 V amplitude, 1.0 μs duration, and 0.15 s interval). The insets show enlarged voltage and current profiles during applying 10 stimulation pulses. (d) Time evolution of the normalized current levels obtained after applying N stimulation pulses (N = 5, 20, 40, and 50) with fixed amplitude (2.5 V), duration (1.0 μs), and interval (0.15 s). The bottom panels show the decay time constant (τ) and the stable synaptic weight (I_0) as functions of the stimulation pulse number, which were determined from the fitting of each curve in the top panel.

stimulation voltage pulses cannot increase the current level of the Ag/PZT/LSMO device at the upward polarization. This indicates that Ag ion migration in the thin PZT film is strongly affected by polarization bound charges at the interfaces. Especially, a gradual increase in the current level at the downward polarization closely resembles the learning effect in human memory, such as a gradual increase in the synaptic weight.[35] In our selectively activated synaptic device, ferroelectric polarization may provide an efficient means of preventing crosstalk between adjacent devices and reconfiguring neural circuits, which is known as the role of astrocyte in neurons.[10−13]

The synaptic weight can be modified by the cooperation of pre- and postsynaptic spikes, and the amount of variation relies on an effective flux, which is determined by the spike parameters, including the pulse amplitude, width, number, and interval. Figure 4c shows the change in the current level of an Ag/PZT/LSMO device with downward polarization, which is caused by consecutive stimulation positive pulses having the (amplitude, duration) of (0.3 V, 0.3 s), (0.35 V, 0.3 s), and (0.4 V, 0.3 s). During the measurement, the total pulse number and pulse interval were fixed at 30 and 12 ms, respectively. Consecutive stimulation induces slow and then sudden change in the current level leading to a final stable one. In other words, the learning effect is most pronounced early in the exponential learning process, and the synaptic weight is reinforced and saturated as the learning process continues, which is consistent with biological phenomena.[1] The applied pulse number, when sudden change in current occurs, decreases as the pulse amplitude increases. The finally obtained current level increases with the pulse amplitude.

As shown in Figure 5a and b, we experimentally demonstrated both volatile and nonvolatile current states in our Ag/PZT/LSMO device to mimic STP and LTP of biological synapse, respectively. For STP, we fixed the amplitude at 2.5 V and the duration at 500 ns of the six applied consecutive stimulation voltage pulses with a long repetition interval of 1.0 s. The Ag/PZT/LSMO device does not maintain a high current level and rapidly returns to a low current value. During the LTP programming, we decreased the pulse repetition interval to 0.15 s while the pulse amplitude and duration were fixed at 2.5 V and 500 ns, respectively. A particular transition to a gradually higher current level is observed with frequently repeated stimulation of input pulses.[4,5,21] Contrary to previous reports, the transition from STP to LTP of our Ag/PZT/LSMO was strongly affected by the direction of ferroelectric polarization: it was only activated at downward polarization of the PZT layer (Supporting

DOI: 10.1021/acs.nanolett.6b05308
Nano Lett. 2017, 17, 1949−1955

Information, Figure S11). We also applied 10 consecutive stimulation voltage pulses with a longer duration of 1.0 μs to our device, while their intervals and amplitudes were maintained at 0.15 s and 2.5 V, respectively. As shown in Figure 5c, a long-lived transition to a higher current level is achieved after the last input pulse, which corresponds to LTP.[8]

The conductance of previously reported synapses was improved by repeated stimulation voltage pulses, and its decay time increased with the number of stimulation pulses.[3−5] To investigate the decay time depending on the stimulation pulse number, we applied N stimulation pulses (N = 5, 20, 40, and 50) with a fixed amplitude of 2.5 V, duration of 1.0 μs, and interval of 0.15 s. The top panels in Figure 5d show the time evolutions of normalized current levels obtained after applying N stimulation pulses along with their fitting results using an exponential decay function:[9]

$$I_t = I_0 + A \exp(-t/\tau) \quad (1)$$

where I_t and I_0 represent the current value at time t and that in the stable state, respectively, A is a prefactor, and τ is the decay time constant. When $t < \tau$, the synaptic weight drops rapidly. When $t \gg \tau$, the synaptic weight varies slowly, and I_t approaches I_0. From the fitting curves in Figure 5d, we can determine I_0 and τ, which increase with N (bottom panels of Figure 5d). These phenomena confirm the STP-to-LTP transition in our device.[9] This enhancement in stability by application of input pulses resembles the increase in synaptic connection following frequently repeated stimulation by action potentials found in the biological neural system.[4] Noticeably, our single synaptic FTJ device has similar τ values to those reported in previous papers[9,25] where a longer programming time of 100 μs and a shorter pulse interval of 200 μs than ours were used.[25] Negative bound charges at the Ag/PZT interface are expected to increase the local concentration of positive Ag ions and thus retard the dissolution of Ag conducting filament.

In summary, we implemented an energy-efficient, ultrasmall, and wide-range operating synaptic device by exploiting cation migration in an FTJ device composed of Ag/PZT/LSMO. Furthermore, it revealed a large on/off ratio (10^7) and essential synaptic functions selectively activated by polarization bound charges, resembling reconfigurable learning and memory function of biological systems.

■ ASSOCIATED CONTENT

Supporting Information

The Supporting Information is available free of charge on the ACS Publications website at DOI: 10.1021/acs.nanolett.6b05308.

Detailed methods, additional information, and figures (PDF)

■ AUTHOR INFORMATION

Corresponding Author

*E-mail: baehpark@konkuk.ac.kr).

ORCID

Bae Ho Park: 0000-0003-0928-329X

Notes

The authors declare no competing financial interest.

■ ACKNOWLEDGMENTS

This work was supported by the National Research Foundation of Korea (NRF) grants funded by the Korea government (MSIP) (No. 2013R1A3A2042120, 2015001948, 2011-0030229, and 2013R1A1A2065339) and Nano·Material Technology Development Program through the NRF funded by the MSIP (No. 2016M3A7B4909668).

■ REFERENCES

(1) Li, Y.; et al. Activity-dependent synaptic plasticity of a chalcogenide electronic synapse for neuromorphic systems. *Sci. Rep.* **2014**, *4*, 4906.

(2) Kuzum, D.; Yu, S.; Wong, H. P. Synaptic electronics: materials, devices and applications. *Nanotechnology* **2013**, *24*, 382001.

(3) Yang, R.; et al. Synaptic plasticity and memory functions achieved in a WO_{3-x}-based nanoionics device by using the principle of atomic switch operation. *Nanotechnology* **2013**, *24*, 384003.

(4) Ohno, T.; et al. Short-term plasticity and long-term potentiation mimicked in single inorganic synapses. *Nat. Mater.* **2011**, *10*, 591.

(5) Chang, T.; Jo, S. H.; Lu, W. Short-term memory to long-term memory transition in a nanoscale memristor. *ACS Nano* **2011**, *5*, 7669.

(6) Hasegawa, T.; et al. Learning abilities achieved by a single solid-state atomic switch. *Adv. Mater.* **2010**, *22*, 1831.

(7) Strukov, D. B.; Snider, G. S.; Stewart, D. R.; Williams, R. S. The missing memristor found. *Nature* **2008**, *453*, 80.

(8) Nayak, A.; et al. Controlling the synaptic plasticity of a Cu_2S gap-type atomic switch. *Adv. Funct. Mater.* **2012**, *22*, 3606.

(9) Li, S.; et al. Synaptic plasticity and learning behaviours mimicked through Ag interface movement in an Ag/conducting polymer/Ta memristive system. *J. Mater. Chem. C* **2013**, *1*, 5292.

(10) Min, R.; Santello, M.; Nevian, T. The computational power of astrocyte mediated synaptic plasticity. *Front. Comput. Neurosci.* **2012**, *6*, 93.

(11) Jourdain, P.; et al. Glutamate exocytosis from astrocytes controls synaptic strength. *Nat. Neurosci.* **2007**, *10*, 331.

(12) Piet, R.; Vargova, L.; Sykova, E.; Poulain, D. A.; Oliet, S. H. Physiological contribution of the astrocytic environment of neurons to intersynaptic crosstalk. *Proc. Natl. Acad. Sci. U. S. A.* **2004**, *101*, 2151.

(13) Smith, K. Neuroscience: Settling the great glia debate. *Nature* **2010**, *468*, 160.

(14) Chanthbouala, A.; et al. A ferroelectric memristor. *Nat. Mater.* **2012**, *11*, 860.

(15) Yamada, H.; et al. Giant electroresistance of super-tetragonal $BiFeO_3$-based ferroelectric tunnel junctions. *ACS Nano* **2013**, *7*, 5385.

(16) Kim, D. J.; et al. Ferroelectric tunnel memristor. *Nano Lett.* **2012**, *12*, 5697.

(17) Wang, Z.; et al. Compact modelling of ferroelectric tunnel memristor and its use for neuromorphic simulation. *Appl. Phys. Lett.* **2014**, *104*, 053505.

(18) Du, N.; et al. Single pairing spike-timing dependent plasticity in $BiFeO_3$ memristors with a time window of 20 to 125 ms. *Front. Neurosci.* **2015**, *9*, 227.

(19) Liu, Q.; et al. Controllable growth of nanoscale conductive filaments in solid-electrolyte-based ReRAM by using a metal nanocrystal covered bottom electrode. *ACS Nano* **2010**, *4*, 6162.

(20) Celano, U.; et al. Three-dimensional observation of the conductive filament in nanoscaled resistive memory devices. *Nano Lett.* **2014**, *14*, 2401.

(21) Waser, R.; Aono, M. Nanoionics-based resistive switching memories. *Nat. Mater.* **2007**, *6*, 833.

(22) Wang, Z.; et al. Memristors with diffusive dynamics as synaptic emulators for neuromorphic computing. *Nat. Mater.* **2016**, *16*, 101.

(23) Terabe, K.; Hasegawa, T.; Nakayama, T.; Aono, M. Quantized conductance atomic switch. *Nature* **2005**, *433*, 47.

(24) Hasegawa, T.; Terabe, K.; Tsuruoka, T.; Aono, M. Atomic switch: Atom/Ion movement controlled devices for beyond Von-Neumann computers. *Adv. Mater.* **2012**, *24*, 252.

DOI: 10.1021/acs.nanolett.6b05308
Nano Lett. 2017, 17, 1949−1955

(25) La Barbera, S.; Vuillaume, D.; Alibart, F. Filamentary switching: synaptic plasticity through device volatility. *ACS Nano* **2015**, *9*, 941.
(26) Wen, Z.; et al. Ferroelectric-field-effect-enhanced electroresistance in metal/ferro-electric/semiconductor tunnel junctions. *Nat. Mater.* **2013**, *12*, 617.
(27) Liu, Qi.; et al. Real-time observation on dynamic growth/dissolution of conductive filaments in oxide-electrolyte-based ReRAM. *Adv. Mater.* **2012**, *24*, 1844.
(28) Yang, Y.; et al. Electrochemical dynamics of nanoscale metallic inclusions in dielectrics. *Nat. Commun.* **2014**, *5*, 4232.
(29) Tsuruoka, T.; Terabe, K.; Hasegawa, T.; Aono, M. Forming and switching mechanisms of a cation-migration-based oxide resistive memory. *Nanotechnology* **2010**, *21*, 425205.
(30) Celano, U.; et al. Understanding the dual nature of the filament dissolution in conductive bridging devices. *J. Phys. Chem. Lett.* **2015**, *6*, 1919.
(31) Gruverman, A.; et al. Tunneling electroresistance effect in ferroelectric tunnel junctions at the nanoscale. *Nano Lett.* **2009**, *9*, 3539.
(32) Brinkman, W. F.; Dynes, R. C.; Rowell, J. M. Tunneling conductance of asymmetrical barriers. *J. Appl. Phys.* **1970**, *41*, 1915.
(33) Choi, S. J.; et al. Improvement of CBRAM resistance window by scaling down electrode size in pure-GeTe film. *IEEE Electron Device Lett.* **2009**, *30*, 120.
(34) Jiang, Lu.; et al. Tunneling Electroresistance induced by interfacial phase transitions in ultrathin oxide heterostructures. *Nano Lett.* **2013**, *13*, 5837.
(35) Wang, Z. Q.; et al. Synaptic learning and memory function achieved using oxygen ion migration/diffusion an amorphous InGaZnO memristor. *Adv. Funct. Mater.* **2012**, *22*, 2759.

DOI: 10.1021/acs.nanolett.6b05308
Nano Lett. 2017, 17, 1949−1955